

# Service Life Testing of Railroad Bearings with Known Subsurface Inclusions: Detected with Advanced Ultrasonic Technology

C.M. Tarawneh<sup>1</sup>, J.A. Turner<sup>2</sup>, L. Koester<sup>2</sup> and B.M. Wilson<sup>3</sup>

<sup>1</sup>Mechanical Engineering Department  
University of Texas-Pan American, Edinburg, Texas

<sup>2</sup>Mechanical and Materials Engineering Department  
University of Nebraska, Lincoln, Nebraska

<sup>3</sup>Research and Development  
Amsted Rail, Granite City, Illinois

## Abstract

Steel cleanliness is of the utmost importance in the production of tapered roller bearings used in the railroad industry. Impurities in the steel can make it vulnerable to fatigue initiation because they act as stress concentration sites in the fabricated parts, especially when these impurities are located in regions of susceptibility for rolling contact fatigue (RCF). Impurities present near the rolling surfaces (*e.g.*, raceways in bearings) are referred to as subsurface inclusions. These subsurface inclusions make the steel susceptible to the initiation of fatigue cracks that can propagate towards the surface leaving a cavity called a “spall”. Spalls occurring on the rolling surfaces of bearings can have detrimental effects that may lead to overheated bearings, loss of full service life, and in extreme cases, can lead to derailments if not addressed in-service by early detection methods. The study presented in this paper investigates the effects of subsurface inclusions present beneath the surface of the bearing cup (outer ring) and cone (inner ring) raceways.

New bearing components were scanned using a unique ultrasonic technique in order to detect and identify potentially detrimental subsurface inclusions present in the RCF regions of the rolling surfaces. Two service life tests of these components were then carried out: one to examine subsurface inclusions found on cone raceways, and one to explore subsurface inclusions present on cup raceways. The test results indicate that the service life of components containing subsurface inclusions is reduced compared to controls for which no subsurface inclusions were detected. Moreover, subsurface inclusions on bearing cups appear to accelerate spall development relative to those present in bearing cones. This paper summarizes the findings of the experimental study performed on ultrasonically scanned bearing components, and emphasizes the need to establish more refined methods to inspect railroad rolling stock. These results are anticipated to be of great value to fatigue life prediction models relevant to the railroad industry.

**Keywords:** service life testing of bearings, rolling contact fatigue, subsurface inclusions, steel cleanliness, advanced ultrasonic technology

# 1 Introduction and background

Roller bearings sustain the heavy loads that railcars can often encounter in coal and consumer goods transport in the heavy haul rail industry. Tapered-roller bearings contain two inner rings (cones) and one outer ring (cup) with rollers transferring the load between the two. In an operational setting, cups are supported on one side by the pedestal of the side-frame, and are known to rotate or 'index' incrementally during service. The load path through the bearing travels between the cups and cones through the rollers. Because cups are fixed, the top hemisphere of the cup is constantly under load, and this region is referred to as the 'loaded zone.' Cones rotate in unison with the wheels and axle and, thus, undergo cyclic loading as regions enter and exit the loaded zone.

Improper assembly, maintenance, or microstructure control can lead to a reduction in the life of the bearing relative to its design specifications. Of particular importance to this paper is the presence of non-metallic inclusions in the steel, which although they can be minimized, they are inherent to the processes used to make steel. If these inclusions occur in the rolling contact fatigue (RCF) zones, then they are termed 'near surface' inclusions.

Based on Hertzian contact mechanics, the highest principal stresses occur at the surface, but they are compressive in nature. However, as a result of the mechanics of contact loading, the maximum shear stress exists at a point below the rolling surface. This stress, which acts to initiate fatigue, will reach a maximum at a depth beneath the surface based on the geometry between the two raceways. For example, the RCF zone in the cups and cones used in this work obtain maximum shear stresses at approximately 200  $\mu\text{m}$  (0.008 in.) from the contact surface [1]. Inclusions located in this area act as stress risers that elevate the local stress in the steel surrounding the impurity to values well above the endurance limit of the steel. This effect can cause micro-cracks to initiate and propagate such that they can eventually reach the surface of the part. This damaged region of the surface is termed 'spalling' in bearings, and additional rolling cycles will cause the bearing to degrade over time.

Ultrasonic scans of metallic materials can be used to determine the inclusion content, material properties, and even applied or residual stresses. Non-metallic inclusions are often inevitable in alloyed materials and their adverse effects on fatigue life have been observed by researchers [2-5]. Consistent with this, a number of industrial standards have been developed for the evaluation of inclusion content in steel using both ultrasonic and optical methods [6-10]. In practice, inclusions are generally identified and rated using either ASTM standard E45 [7] or ISO 4967 [10], whereby both standards outline procedures and techniques for assessing the size and density of four specific types of inclusions. A typical inclusion evaluation is performed by first sampling a section of the material in question. This sample is then examined to determine the worst visual area of inclusions microscopically, which is meant to serve as a representation of the steels' bulk quality. However, a limitation of this process is that only a small area relative to the entire volume of the heat or section is actually examined, yet the examined area is assumed to be representative

of the bulk material. As an example, two C-scans of certified ‘Bearing Quality Steel’ are shown in Figure 1. Clearly these two steels would perform very differently if or when they were manufactured into bearings.



Figure 1: C-scans of two bearing steels which have both been certified and rated as ‘Bearing Quality’ based on microscopic rating methods

Even with the reduction of overall inclusion content through quality measures based on optical and bulk ultrasonic inspections of bearing steels, the possibility still exists for an inclusion to be present in near-surface regions with high RCF induced stresses. Therefore, bulk inspection methods have limited success in identifying where problematic inclusions will exist relative to the rolling race, despite having the ability to improve overall steel quality. This concern has led to advancements in steel production methods and quality specifically for bearings as well as the rail industry in general [5, 11]. However, in order to advance these techniques even further, the development of technology that can focus on identifying inclusions in the RCF zone of the bearing is the next logical step in the advancement of producing true bearing quality steels with zero near-race defects.

The technique explored in this paper is to scan the bearing components by using ultrasonic surface waves. Surface acoustic waves have the unique property that they propagate along free surfaces through a depth of approximately one acoustic wavelength (of the order of hundreds of microns at moderate frequencies in structural materials, *i.e.* steel, aluminum, *etc.*). In this article, bearing cups and cones are scanned using a calibrated surface wave scanning method to take advantage of this phenomenon. Bearings with known near-surface defects are identified and subjected to simulated service life testing. Spall locations and ultrasonic surface wave scanning results are compared to examine the capability of using surface wave ultrasonic testing for identifying potential spall initiation sites.

## 2 Bearing component selection for service life testing

Selection of the bearing components to undergo service life testing was carried out at Amsted Rail's bearing division, Brenco, using their ultrasonic inspection system which utilizes a surface wave approach described previously [12]. A total of fifty bearing cups (outer rings) and forty cones (inner rings) were ultrasonically scanned, out of which twelve cones and three cups were identified for possible service life testing. The components were then retested at the University of Nebraska-Lincoln (UNL) to verify the results, and to identify any indications that may have been missed in the initial scanning. Surface wave scanning was performed with scan resolutions and pulser settings chosen to minimize beam overlap and maximize reflection from a laser machined hole of 60  $\mu\text{m}$ . The inspection volume is limited to within one wavelength of the material surface ( $\sim 200 \mu\text{m}$ ), which can be calculated using the testing frequency (15 MHz) and the Rayleigh wave speed. The 200  $\mu\text{m}$  scanning depth was chosen based on the work done by Dick and Wilson [1] which provides validated computational models that determine the individual roller loads and the Hertzian contact stress in railroad bearings.

The results from the ultrasonic surface wave scanning performed at UNL on both the cups (outer rings) and cones (inner rings) are summarized in Table 1 and Table 2, respectively. These tables list the locations of the near-surface inclusions identified in each of the three cups and eight cones chosen for service life testing, in terms of their vertical ( $z$ ) and circumferential ( $\theta$ ) position. In the case of the cones, the inclusions are referenced from the starting position, marked on the small rim of the cone, in a clockwise manner when viewed from the small rim of the cone. For the cups, the  $z$ -location is referenced from the start of the undercut in the axial direction for both the inboard and outboard raceways, whereas, the  $\theta$ -location is referenced as shown in Figure 2.

Test Cup	Outboard (OB)/ Inboard (IB)	$\theta$ [deg]	$z$ [mm]
A	OB	-	-
	IB	244.1	26.2
B	OB	135.7	31.2
	IB	-	-
C	OB	264.3	32.7
	OB	66.5	4.4
	IB	99.4	35.0
	IB	294.8	6.4

Table 1: Circumferential ( $\theta$ ) and vertical ( $z$ ) positions of the subsurface inclusions found in the three bearing cups (outer rings) selected for service life testing

Cone No.	$\theta$ [deg]	$z$ [mm]	Cone No.	$\theta$ [deg]	$z$ [mm]
2	151.0	29.0	14	257.0	10.5
10	225.5	4.5	16	36.5	34.0
	337.5	26.5		292.0	4.0
24	215.5	23.5	5	72.0	30.5
	237.5	5.0		129.0	37.0
	314.0	36.5		151.0	8.0
				240.5	23.5
32	103.0	23.0	31	79.5	21.5
	104.5	17.5		195.5	28.0
	117.0	35.5		257.5	40.5
	248.5	28.5		265.0	32.0
	117.0	35.5		273.0	9.5

Table 2: Circumferential ( $\theta$ ) and vertical ( $z$ ) positions of the subsurface inclusions found in the eight bearing cones (inner rings) selected for service life testing

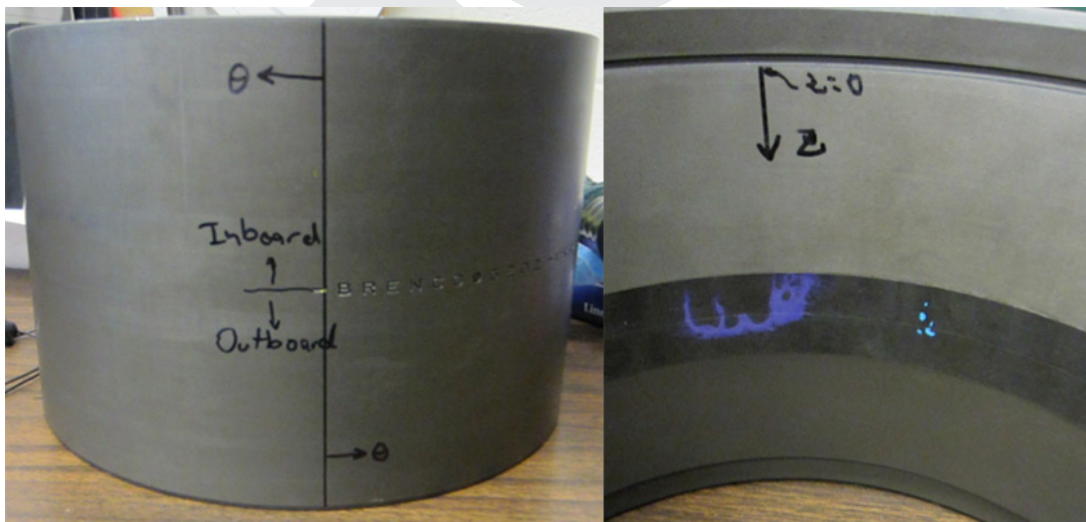


Figure 2: Photographs of the bearing cup (outer ring) showing the reference points for the circumferential ( $\theta$ ) and vertical ( $z$ ) coordinates for the inboard (IB) and outboard (OB) raceways

Figure 3 is a representative scan image from the UNL ultrasonic surface wave scanning system (degrees and mm) for Test Cup C. The high amplitude indications along the top and bottom of the UNL scan image should be ignored as they represent the edges of the raceways. Finally, it should be noted that clean (defect-free) cups were used in the service life testing of cones with subsurface inclusions, and clean cones were used in the service life testing of cups with near-raceway inclusions. The latter was done in an effort to isolate the chance of premature failure to the bearing components that contain subsurface inclusions in the raceways. Rollers and other bearing components were not inspected for subsurface inclusions. In total, eight cones (inner rings) and three cups (outer rings) were used to carry out two consecutive service life tests utilizing the dynamic four-bearing test rig at the University of Texas-Pan American (UTPA). For brevity, the work presented here will mainly focus on the service life testing performed on the bearing cups as the earlier study conducted on the bearing cones has been published elsewhere [13]. However, a summary of the main results from the service life testing of cones (inner rings) is also provided.

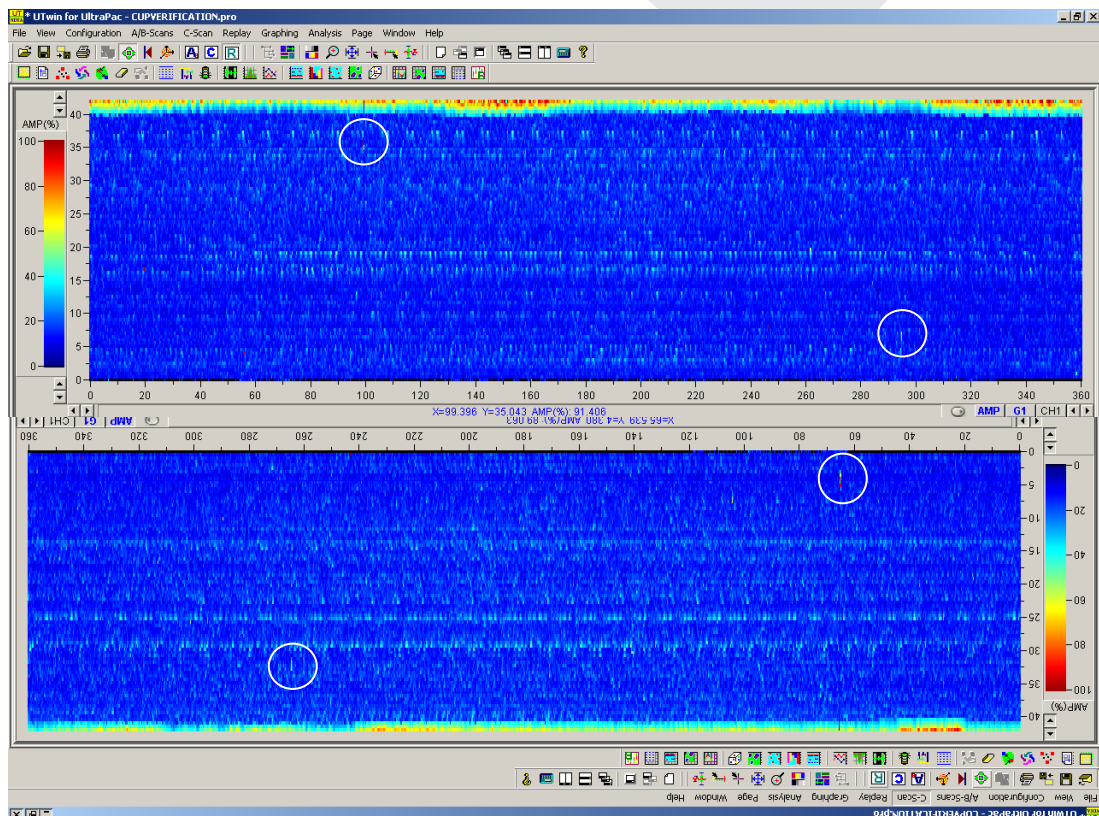


Figure 3: A scan image of the inspection performed on Test Cup C which indicates the presence of four distinct sub-surface inclusions on the inboard (top) and outboard (bottom) raceways [Refer to Table 1]

### 3 Experimental setup and instrumentation

The service life tests were performed using the dynamic bearing tester at UTPA depicted in Figure 4. The dynamic test rig can accommodate four Class K ( $150 \times 250$  mm) tapered-roller bearings mounted on a customized axle, courtesy of Amsted Rail. Depending on the size of the pulley used, the axle can be rotated at four different angular velocities of 498 r/min, 562 r/min, 618 r/min, and 794 r/min which correspond to train speeds of approximately 85.3 km/h (53 mph), 96.6 km/h (60 mph), 106.2 km/h (66 mph), and 136.8 km/h (85 mph), respectively. Cooling was achieved with three fans that produced an air stream traveling at an average speed of 5 m/s (11.2 mph). The dynamic bearing tester is equipped with a hydraulic cylinder capable of applying loads ranging from 0 to 175% of full load [100% load condition simulates a fully-loaded railcar and corresponds to a load of 159,000 N (35,750 lb) per bearing]. In an effort to accelerate the service life test, the bearings were tested at 136.8 km/h (85 mph) utilizing a load setting of 125% of full-load for the majority of the test duration. A 17% load setting, simulating an empty railcar, was used in cold starts at which time the bearing grease is more viscous. This procedure was used in order to avoid overloading the motor.

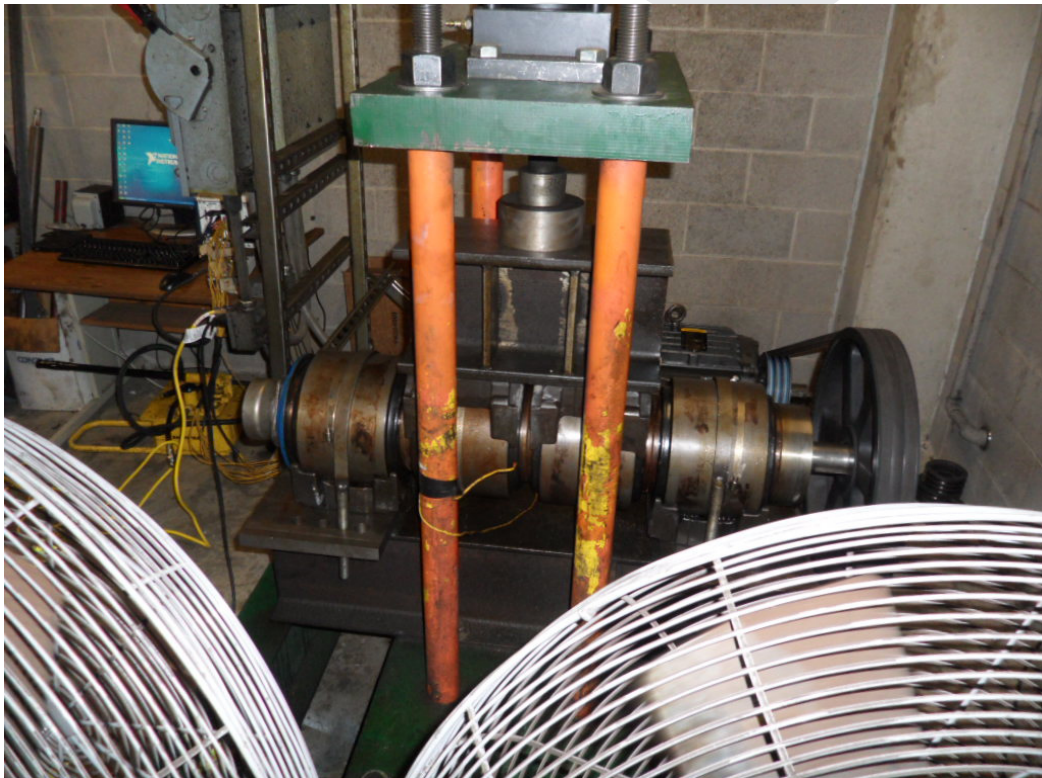


Figure 4: Photograph of the dynamic bearing tester used to conduct the service life test for this study

The instrumentation setup is illustrated in the schematic shown in Figure 5. Four bearing adapters were specially machined to accept an accelerometer and two



## 4 Experimental procedure

Table 3 describes the bearing setup on the dynamic test rig indicating the location of the ultrasonically scanned cups on the axle assembly illustrated in Figure 5. Because only three cups were scanned, a fourth control (defect-free) bearing was used to complete the axle setup. For Bearings 2 and 4, the near-surface inclusion sites (listed in Table 1) were placed in the region of maximum load (12 o'clock) within the loaded zone of the outer ring (cup). In the case of Bearing 3, which presented multiple subsurface indications, the inclusions on the OB  $\sim 264^\circ$  and IB  $\sim 99^\circ$  were placed in the loaded zone (around 12 o'clock), leaving the other two inclusions in the unloaded region of the cup (bottom hemisphere).

Bearing Location	Test Cup [Setup Before First Teardown]	Test Cup [Setup After First Teardown]
B1	Control (Defect-Free) Cup	Control (Defect-Free) Cup
B2	B	C
B3	C	B
B4	A	A

Table 3: Bearing setup on the dynamic test rig showing the location of the ultrasonically scanned cups on the axle assembly (refer to Figure 5)

Once the bearings were instrumented with thermocouples and accelerometers, the load was applied via the hydraulic cylinder. Then, the data acquisition system was initiated, and the motor was started. Following the break-in period (17 % of full-load), the load setting was increased to 125% of full-load (100% load equivalent is equal to 35,750  $lb_f$  for an AAR Class K bearing) while the axle speed was maintained at 136.8 km/h (85 mph). The latter settings were maintained for the majority of the service life test. Lower loads were utilized only in cold starts after the tester has been off for any period greater than twelve hours.

The test plan was developed to allow the service life test to run uninterrupted while the temperature and vibration signatures of the four bearings were monitored. If either the temperature history or the vibration signal indicates an abnormal bearing operation [14], the test was to be stopped so that the bearing can be disassembled and visually inspected. Once a thorough inspection has been performed, the bearing is rebuilt, and the test resumed while the total distance traveled was recorded. This process was to be repeated until the bearings have been cycled for an equivalent of at least 402,336 km (250,000 mi), which represents a typical benchmark for simulated service life testing. Note that a typical service life test takes anywhere from 6 to 9 months to complete depending on the number of teardowns and inspections performed. The size of these railroad bearings and the relatively large applied loads prohibits the type of accelerated life testing usually performed on much smaller size ball bearings.

## 5 Experimental results

The temperature profiles and vibration signatures of all four bearings on the axle assembly were closely monitored throughout the service life test for signs of abnormal behaviour. The first of such signs was observed in Bearing 3 which, over the last five hours of the test, exhibited an increase in temperature at a relatively higher rate than the other three bearings, as seen in Figure 6. The latter, coupled with the preceding increase in the vibration energy of that specific bearing, was an indication that a defect has initiated. Note that the sudden temperature increase seen around 648 hours is a consequence of a sudden test restart, followed by approximately 30 minutes of the tester running without forced convection before fans were turned on. Changes in temperature observed around 623 hours are a consequence of the test being stopped for setup modifications and then restarted. Data were not collected while the tester was off and fans were turned off to avoid significant cooling of the bearings.

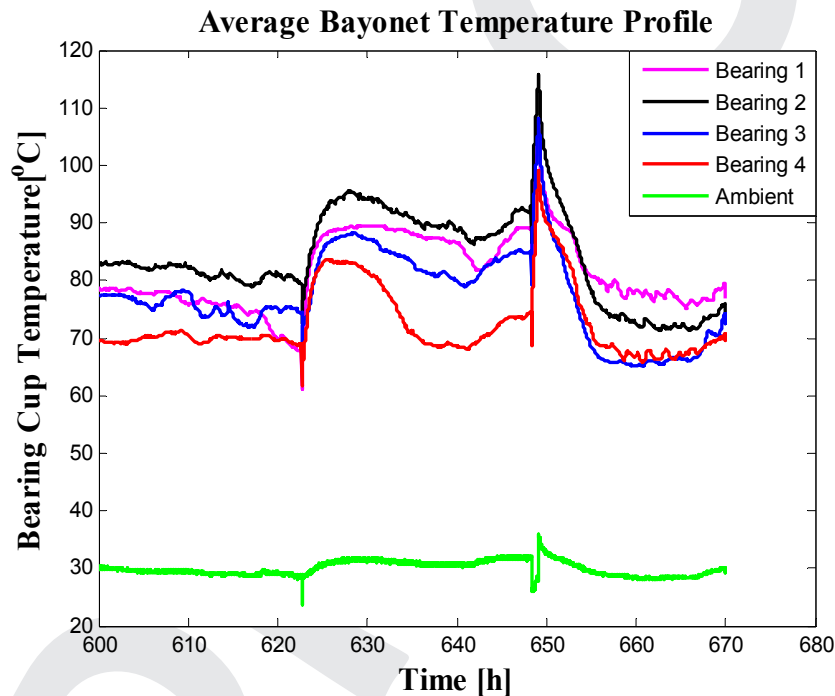


Figure 6: Average temperature profiles of all four bearings prior to the first teardown

Here the temperature profiles are shown because temperature is the primary identifier for degrading bearings in the railroad industry. Alternative methods based on the vibration signature, such as tracking of the vibration energy of a bearing, have been shown to be more effective in certain cases [14], yet this method is not established in the industry. Vibration events usually precede temperature fluctuations, especially when defects develop within the bearing. In this case, after 114,294 km (71,019 mi) of operation, an increase in the vibration energy of Bearing 3 was observed. Consequently, the bearing tester was stopped after running 115,799

km (71,954 mi) to conduct a complete teardown and visual inspection of all four bearings.

## 5.1 First teardown inspection

Upon teardown and inspection of the bearings, a spall was found on the cup outboard (OB) raceway of Bearing 3 (Test Cup C). The spall was located at  $\theta = 264^\circ$ , which matched the  $\theta$  for one of the subsurface indications on the outboard (OB) raceway as detected by the ultrasonic surface wave scans. However, the spall initiated at the top of the raceway ( $z < 20$  mm) and is approximately 16.05 mm long and 9.80 mm wide ( $0.632 \times 0.386$  in.), as shown in Figure 7, a location different from the subsurface inclusion detected at  $z = 32.7$  mm (see Table 1). This spall formed after only 115,799 km (71,954 mi) of bearing operation at 85 mph and 125% load.

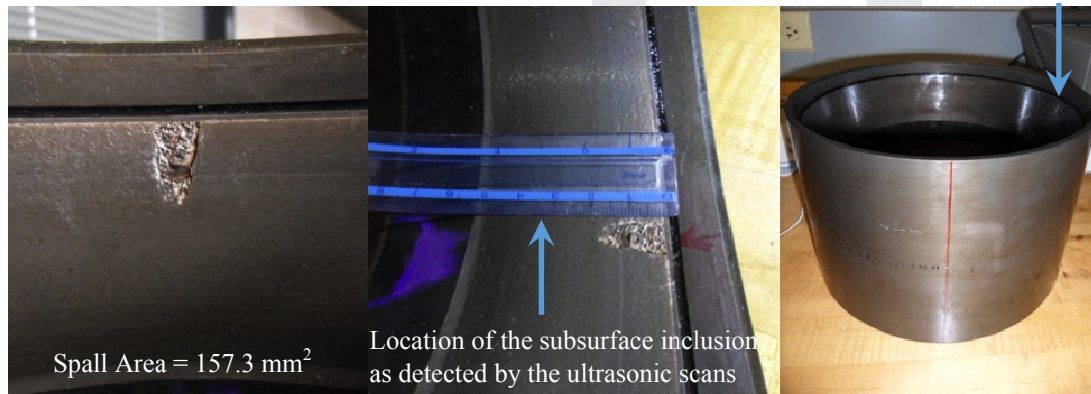


Figure 7: Photographs of the first cup spall that developed on Bearing 3 (Test Cup C) – Teardown 1

After all bearings were carefully inspected for any evidence of spall formation, they were reassembled and testing was resumed. In the case of Bearings 2 and 4, which had not developed a spall, they were positioned as they were before the teardown; that is, with the detected near-surface inclusions at the region of maximum load. As for Bearing 3 (Test Cup C), the outer ring (cup) was indexed so that the other two detected subsurface inclusions, which had not spalled yet, were in the region of full load leaving the spalled region in the unloaded zone of the cup. Additionally, the location of Bearings 2 and 3 (both top-loaded) were exchanged in order to verify that the vibration energy of each bearing is independent of the location on the test axle assembly. The new bearing setup is provided in Table 3.

Upon continuation of the service life test, temperature and vibration of all four bearings were closely monitored. The large temperature increases and decreases seen in Figure 8 are a direct consequence of sudden changes in load or short period test stoppages. Bearing temperatures varied greatly throughout the experiment; Bearing 2 (Test Cup C), previously Bearing 3, occasionally displayed temperatures

higher than the other three bearings, including the last ten hours of the experiment. Moreover, the vibration energy of Bearing 2 exhibited a discernible increase after running for 118,897 km (73,879 mi). Consequently, the bearing tester was stopped after a total of 238,260 km (148,048 mi) of operation to perform a second teardown and inspection of all bearings.

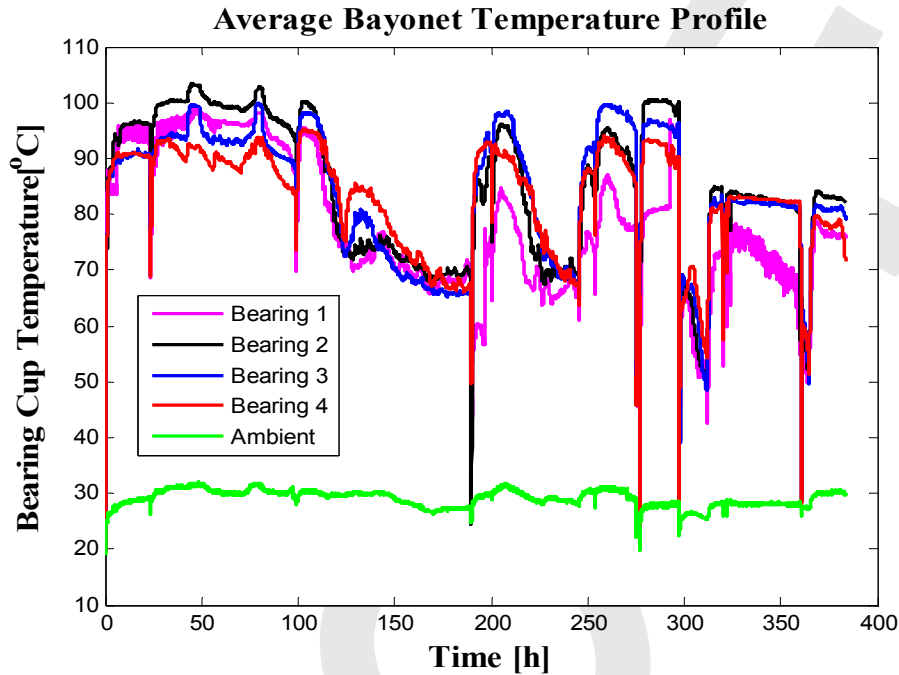


Figure 8: Average temperature profiles of all four bearings after the first teardown and prior to the second teardown

## 5.2 Second teardown inspection

Upon teardown and inspection of the test bearings, the existing spall on Bearing 2 (Test Cup C) was found to have deteriorated significantly. The spall, located at  $\theta = 264^\circ$ , now had a maximum length of 36.42 mm and a maximum width of 9.39 mm, which constitutes an increase in the spall area from 157.3 mm<sup>2</sup> in the first teardown to 237.87 mm<sup>2</sup> in the second teardown. The new spall length now coincides with the subsurface inclusion location ( $z = 32.7$  mm, see Table 1). An important observation from the deteriorated spall, shown in Figure 9, is that the initial spall area is deeper into the raceway than that of the spall growth area. This result is not surprising given the fact that the initial spall developed while under maximum load, whereas, the deterioration occurred with the spall positioned in the unloaded region of the outer ring (cup).

Visual inspection of the other three bearings did not reveal any defects or spalls. Thus, the bearings were rebuilt, pressed on the axle following the same exact configuration as that prior to the second teardown, and the service life test was resumed.

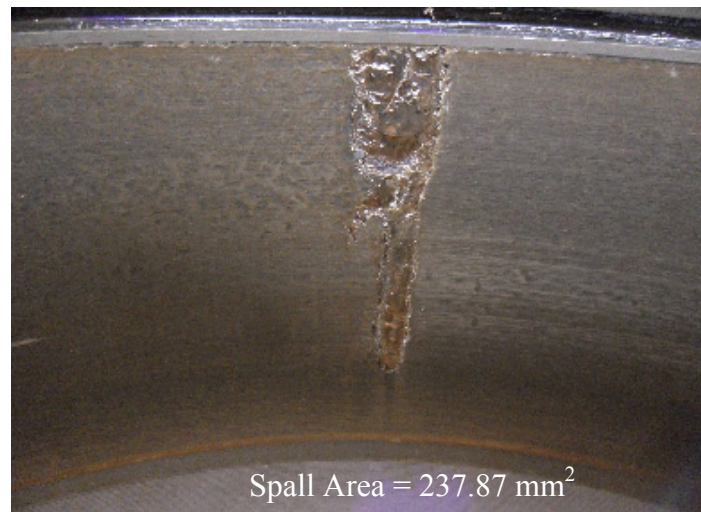


Figure 9: Photograph of the cup spall on Bearing 2 (Test Cup C) after deterioration – Teardown 2

Upon continuation of the service life test, it was noticed that the temperature of the defective Bearing 2 (Test Cup C) was now consistently higher than the defect-free bearings, as can be seen in Figure 10. Furthermore, shortly after the test was resumed for an additional 20,500 km (12,738 mi), a significant increase in the vibration energy of Bearing 2 was detected, suggesting further deterioration of the existing spall. Consequently, the bearing tester was stopped after a total of 262,604 km (163,174.5 mi) of operation to carry out a third teardown and inspection of all test bearings.

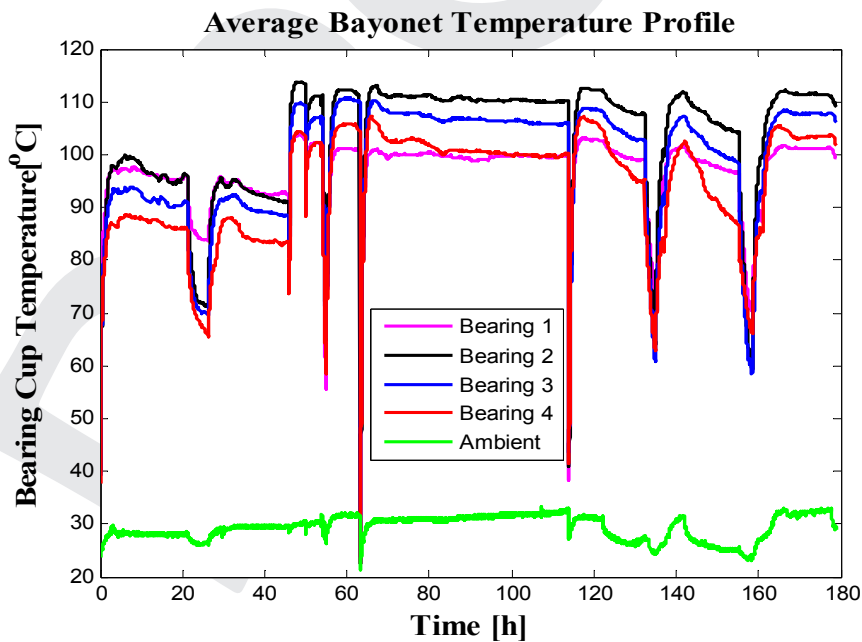


Figure 10: Average temperature profiles of all four bearings after the second teardown and prior to the third teardown

### 5.3 Third teardown inspection

Upon teardown and visual inspection of the bearings, the existing spall on Bearing 2 (Test Cup C) was found to have deteriorated further. While the maximum length and width of the spall remained the same as in the second teardown, the wider region of the spall increased in length, thus, changing the total area of the spall from 237.87 mm<sup>2</sup> to 261.42 mm<sup>2</sup>, as shown in Figure 11.



Figure 11: Photographs of the cup spall on Bearing 2 (Test Cup C) after second sign of deterioration – Teardown 3

Once again, the bearings were rebuilt, pressed onto the axle following the same setup as before the third teardown, and the test resumed. After a total of 288,074 km (179,001 mi) of operation, the temperature and vibration data of Bearing 2 (Test Cup C) exhibited a noticeable increase. Therefore, the bearing tester was stopped, and a complete visual inspection of all test bearings was performed.

### 5.4 Fourth teardown inspection

Upon teardown and visual inspection of the bearings, a new spall was found on the inboard (IB) cup raceway of Bearing 2 (Test Cup C). The new spall was located at  $\theta = 295^\circ$ , which matched the  $\theta$  for one of the near-surface inclusions on the IB raceway as detected by the ultrasonic surface wave scans (see Table 1). The spall was approximately 20.85 mm long and 5.26 mm wide (0.821 × 0.207 in.), as shown in Figure 12, and coincided perfectly with the subsurface inclusion detected at  $z = 6.4$  mm.

Upon close inspection of Bearing 3 (Test Cup B), the initial stages of spall formation were observed at the exact location of the near-surface inclusion detected by the ultrasonic wave scans (see Table 1). The size of the defect was very small at this stage, as shown in Figure 13. The bearing was reassembled and mounted onto the axle with the spall location placed directly under the region of maximum load (top hemisphere, 12 o'clock). The bearing/axle assembly setup was identical to that used prior to the fourth teardown. The test was resumed again and Bearings 2 and 3 were closely monitored.

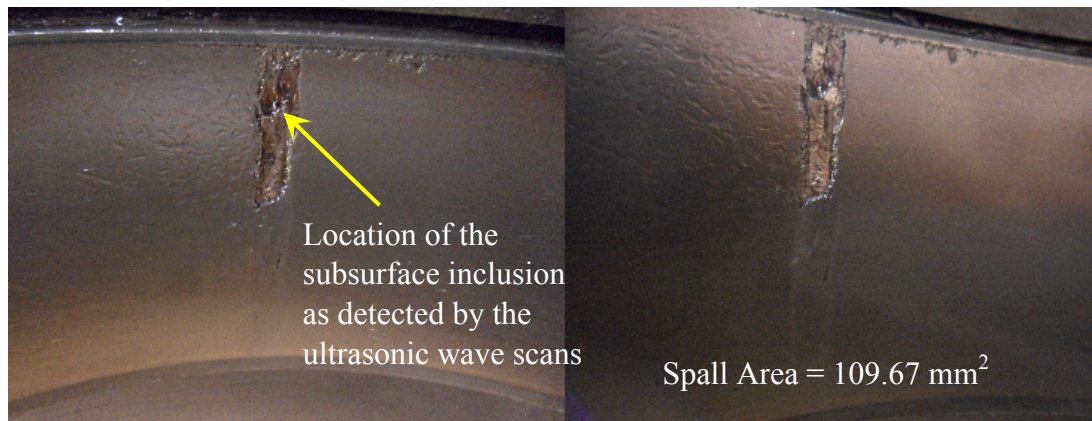


Figure 12: Photographs of the second cup spall that developed on Bearing 2 (Test Cup C) – Teardown 4

Following the fourth teardown, the bearings were run past the 402,336 km (250,000 mi) milestone completing 420,729 km (261,429 mi) of total service. The bearing temperature profiles for the last 515 hours of testing are provided in Figure 14. Note that bearing operating temperatures rarely dropped below 70°C. Similar to the temperature profiles shown previously, sudden temperature drops and increases are a consequence of short duration stops followed by restarts. The temperatures of Bearings 2 and 3 ran consistently hot and remained close to 100°C levels. However, what raised concerns was the fact that the temperature of Bearing 4 (Test Cup A) started approaching the same levels of Bearings 2 and 3 over the last 24 hours of the test coupled with a significant increase in its vibration energy.



Figure 13: Photograph of the initial stage of cup spall formation on Bearing 3 (Test Cup B) – Teardown 4

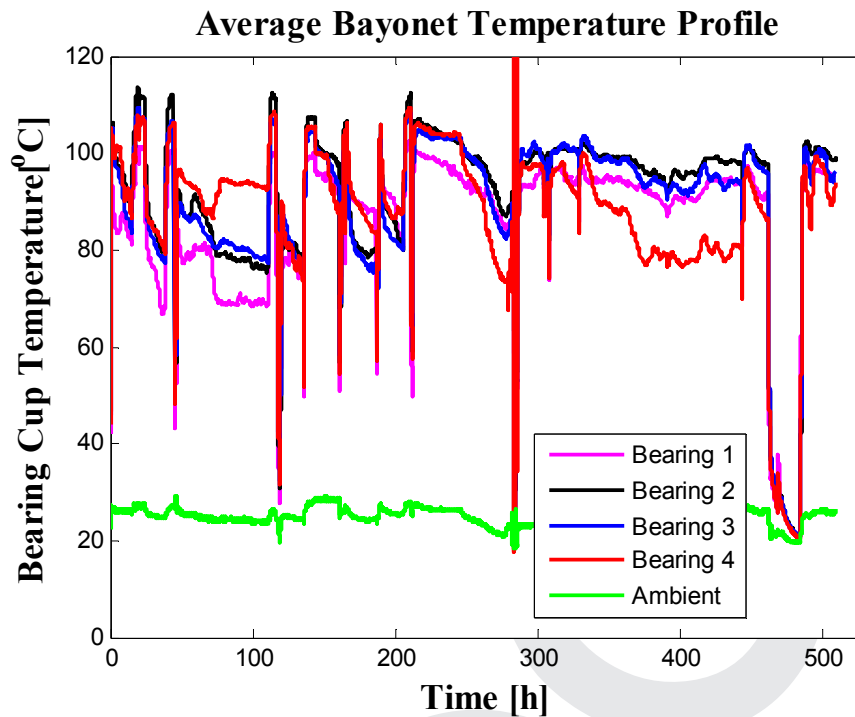


Figure 14: Average temperature profiles of all four bearings after the fourth teardown and prior to the fifth and final teardown

The increase in the vibration energy of Bearing 4 (Test Cup A) was detected after 415,394 km (258,114 mi) of operation. A similar increase in energy was also observed in Bearing 3 (Test Cup B). The latter behaviour coupled with the visible increase in the temperature of Bearing 4 and the fact that the total test mileage exceeded the 402,336 km (250,000 mi) milestone prompted the fifth and final teardown and inspection of all four bearings involved in this service life test.

## 5.5 Fifth and final teardown inspection

Upon final disassembly and visual inspection of all four bearings involved in the service life test, the following observations were made.

### 5.5.1 Bearing 1 (Defect-Free Cup)

This control bearing was scanned for subsurface inclusions and was determined to be a defect-free (healthy) bearing at the start of the service life test. After running a total of 420,729 km (261,429 mi) in the service life test, this bearing did not exhibit any signs of defects or abnormalities. The latter fact is also supported by this bearing's operating temperature which ran lower than the other three bearings the majority of the test, and its vibration energy levels which were the lowest of all bearings throughout this service life test.

### 5.5.2 Bearing 2 (Test Cup C)

Two main observations were made upon inspection of this bearing; the area of the second cup spall (Spall 2) increased significantly to  $933.83 \text{ mm}^2$ , which corresponds to a length of 48.26 mm and a width of 19.35 mm ( $1.9 \times 0.762 \text{ in.}$ ), as shown in Figure 15. By comparing it to the size of this spall from the previous teardown ( $109.67 \text{ mm}^2$ ), Spall 2 grew eight and a half times its original area in approximately 117,285 km (72,878 mi) of operation. Moreover, one of the rollers on the cone assembly corresponding to the cup raceway containing Spall 2 was found to have formed two significant spalls, as shown in Figure 15. It was also observed that the majority of the rollers on both cone assemblies of Bearing 2 exhibit signs of minor pitting, probably resulting from the small pieces of steel coming off the spalled raceways and roller. The area of Spall 1 did not experience any noticeable increase in size, which is not surprising considering this spall was positioned in the unloaded region (bottom hemisphere, 6 o'clock) of the bearing as opposed to Spall 2 which was placed directly under the maximum load region (top hemisphere, 12 o'clock).

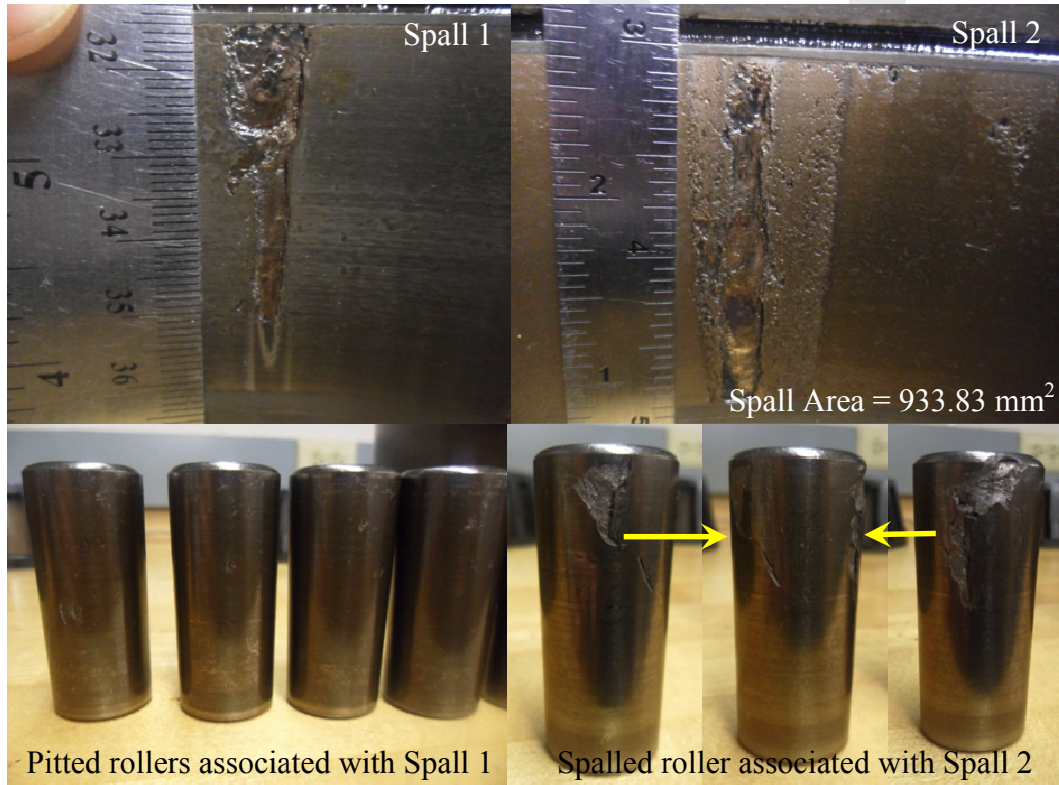


Figure 15: Photographs of Spall 1 (left) and Spall 2 (right) on Bearing 2 (Test Cup C) and the condition of the associated rollers upon final inspection – Teardown 5

### 5.5.3 Bearing 3 (Test Cup B)

Upon inspection of Bearing 3, the region of the cup raceway which exhibited an initial stage of spall formation (see Figure 13) remained unchanged from the

previous teardown, and no other spalls were found on the cup raceways. However, the vibration energy of this particular bearing was relatively high compared to that of a defect-free (healthy) bearing (Bearing 1). Moreover, the operating temperature of this bearing was among the highest for the majority of the service life test. A closer look at the rollers of both cone assemblies from this bearing revealed an abnormal discoloration resembling a distinct heat tint (see Figure 16) likely caused by the excessive heat generation within this bearing. This behavior is typical of temperature-trended bearings in which the high levels of vibration energy within the bearing tend to induce frequent roller misalignment, which in turn causes some of these rollers to be caught misaligned as they enter the loaded region of the bearing, thus, generating excessive frictional heating through roller skidding [15]. The aforementioned statement is further validated by the irregular wear patterns visible on both cup raceways of Bearing 3, seen in Figure 16. The figure also demonstrates the roller discoloration observed in the rollers of Bearing 3. The first roller on the left, seen in Figure 16, is a roller from the defect-free (healthy) Bearing 1 which ran the same exact distance as the two rollers on the right, which were taken from the two cone assemblies of Bearing 3.

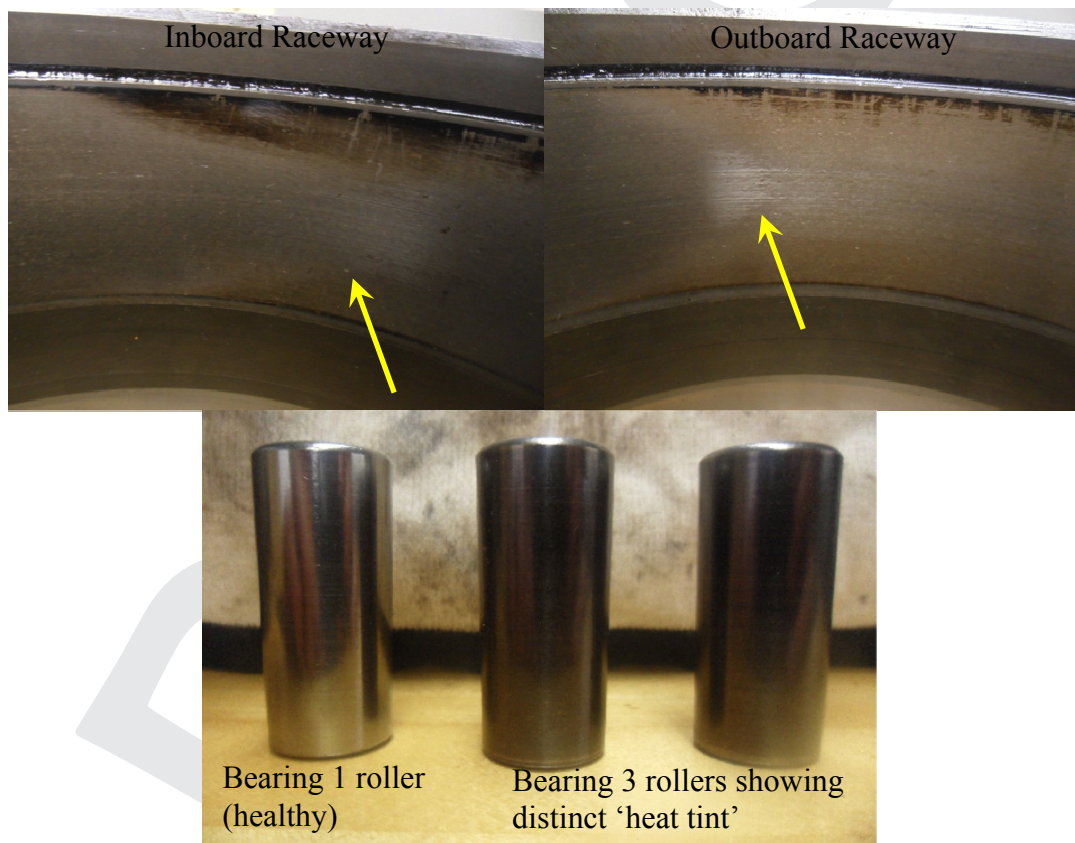


Figure 16: Photographs showing the irregular wear patterns on the inboard and outboard raceways of Bearing 3 (Test Cup B) and a comparison of a roller from Bearing 1 (Healthy) and two rollers from Bearing 3 to demonstrate the “heat tint” discoloration – Teardown 5

#### 5.5.4 Bearing 4 (Test Cup A)

Upon teardown and inspection of Bearing 4, a large spall was found on the inboard (IB) cup raceway. The spall was located at  $\theta = 310^\circ$  as indicated in Figure 17, which did not match the  $\theta$  for the subsurface inclusion on the IB raceway as detected by the ultrasonic surface wave scans ( $\theta = 244.1^\circ$ ). The chosen origin ( $\theta = 0^\circ$ ) in the ultrasonic surface wave scans is shown in Figure 17, and the angle  $\theta$  is measured clockwise from the origin for the IB raceway. The spall size is approximately 36.00 mm long and 25.35 mm wide ( $1.417 \times 0.998$  in.), as seen in Figure 17. More importantly, the spall developed and reached its final area of  $912.6 \text{ mm}^2$  ( $1.414 \text{ in}^2$ ) within only 5,335 km (3,315 mi) of operation. Furthermore, a closer inspection of the cone assemblies revealed that the polyamide cage corresponding to the spalled raceway formed a substantial crack, as shown in Figure 17.



Figure 17: Pictures of the cup spall that developed on Bearing 4 (Test Cup A) and the associated cage damage – Teardown 5

Note that the ultrasonic surface wave scans are sensitive to near-surface inclusions within  $200 \mu\text{m}$  from the surface. The spall that initiated in Bearing 4 was possibly caused by an inclusion that was deeper than the scanned region. For future work, the depth of the scans from the surface needs to be adjusted to capture relevant inclusions that might be a little deeper beyond the Hertzian contact stress region ( $\sim 200 \mu\text{m}$ ). Nonetheless, the rate at which the spall developed and deteriorated in such a short period of operation is yet another example of the importance of steel cleanliness, and underscores the need to use ultrasonic surface wave scans as a quality control tool. The results of the service life tests performed on the ultrasonically scanned cups (outer rings) and cones (inner rings) are summarized in Table 4 and Table 5, respectively.

Teardown Number	Event Description	Test Cup	Defect Size [mm <sup>2</sup> ]	Distance When Energy Increased (Distance since Rebuilding) [km]	Total Distance to Teardown [km]
1	First spall initiated (Spall 1) [OB, $\theta \approx 264^\circ$ , $z < 20$ mm]	C	157	114,294	115,799
2	Area of Spall 1 increased [see Figure 9]	C	238	234,695 (118,897)	238,260
3	Area of Spall 1 increased [see Figure 11]	C	261	258,760 (20,500)	262,604
4	Second spall formed (Spall 2) [IB, $\theta \approx 295^\circ$ , $z = 6.4$ mm]	C	110	288,074 (25,470)	303,444
	Initial stages of spall formation [OB, $\theta \approx 136^\circ$ , $z = 31.2$ mm]	B	~ 4	288,074 (25,470)	303,444
5	<ul style="list-style-type: none"> <li>Area of Spall 2 increased significantly</li> <li>Roller spalls formed [see Figure 15]</li> </ul>	C	934	N/A	420,729
	<ul style="list-style-type: none"> <li>Distinct 'heat tint' discoloration observed on rollers</li> <li>Irregular wear patterns visible on both cup raceways [see Figure 16]</li> </ul>	B	N/A	N/A	420,729
	<ul style="list-style-type: none"> <li>First spall formed (Spall 3) [IB, <math>\theta \approx 310^\circ</math>, <math>z &gt; 25</math> mm]</li> <li>Polyamide cage developed a significant crack on the smaller diameter rim [see Figure 17]</li> </ul>	A	913	415,394 (111,950)	420,729

Table 4: Summary of all teardowns for the ultrasonically scanned bearing cup service life test (performed in 2012)

Teardown Number	Event Description	Test Cone	Defect Size [mm <sup>2</sup> ]	Distance When Energy Increased (Distance since Rebuilding) [km]	Total Distance to Teardown [km]
1	General teardown and inspection of all test bearings	N/A	None	N/A	196,262
2	First spall initiated on Test Cone 5 [ $\theta = 72^\circ$ , $z = 30.5$ mm]	5	70	303,259	319,765
3	Spall on Test Cone 5 deteriorated significantly and spread across the length of the raceway	5	844	354,056 (34,291)	380,002
4	First spall initiated on Test Cone 32 [ $\theta = 104.5^\circ$ , $z = 17.5$ mm]	32	152	373,094 (53,329)	406,394
	First spall initiated on Test Cone 16	16	94	395,072 (15,070)	406,394
5	Area of the spall on Test Cone 32 increased significantly and spread across the length of the raceway	32	405	410,056 (3,662)	420,937
	Rollers associated with Test Cone 32 exhibited signs of pitting	32	N/A	N/A	420,937

Table 5: Summary of all teardowns for the ultrasonically scanned bearing cone service life test (performed in 2011)

## 6 Conclusions and recommendations

The study presented in this paper demonstrates that the existence of near-surface inclusions on the outer ring (cup) raceways promote the initiation of early stage spalling at relatively low mileage, as evident by the first spall formation after only 114,294 km (71,019 mi) of operation for one bearing. Once a spall has formed, it can deteriorate relatively quickly without exhibiting any signs of this deterioration in the temperature history until the spall is large enough to cause significant abnormal operation leading to enhanced metal-to-metal friction, which results in an increase in

the operating temperature of the bearing. The aforementioned observation becomes evident when looking at the spall of Bearing 4 (Test Cup A), which developed and grew to a size of  $912.6 \text{ mm}^2$  ( $1.414 \text{ in}^2$ ) within only 5,335 km (3,315 mi) of operation. Moreover, the second spall that developed in Bearing 2 (Test Cup C) grew in size from  $109.67 \text{ mm}^2$  to  $933.83 \text{ mm}^2$  ( $\sim 8.5$  times the size) in approximately 117,285 km (72,878 mi) of operation.

The service life test conducted on the ultrasonically scanned bearing cones (inner rings) was also successful in demonstrating the detrimental effect of near-surface inclusions. Three cones (Test Cones 5, 32, and 16) initiated spalls after 303,259 km (188,436 mi), 373,094 km (231,830 mi), and 395,072 km (245,486 mi) of operation, respectively, as summarized in Table 5. The spalls that developed on Test Cones 5 and 32 matched exactly the locations of near-surface inclusions as indicated in Table 5, whereas, the spall that initiated on Test Cone 16 matched the  $z$ -location but not the  $\theta$ -location (was off by  $\sim 15^\circ$ ). More importantly, the successive teardowns showed that the spall that developed on Test Cone 5 grew twelve times in size within 60,237 km (37,430 mi) of operation, whereas, the spall on Test Cone 32 nearly tripled in size after only 14,543 km (9,037 mi) of operation. The latter results demonstrate the potential of these spalls to cause catastrophic bearing failure over short periods of operation.

Comparing the results of the two service life tests, it was noticed that the cups (outer rings) developed spalls at the locations of near-surface inclusions much faster than in the case of the cones (inner rings). It took only 114,294 km (71,019 mi) of operation for the first spall to develop on Test Cup C, whereas, it took 303,259 km (188,436 mi) of operation for the first spall initiation on Test Cone 5. The latter is not surprising considering that cones (inner rings) are only loaded 50% of their operational service as they enter and exit the loaded region of the bearing. However, the cups remain stationary for the most part unless they index during service. Thus, if a near-surface inclusion on a cup raceway happens to be in the loaded region of the bearing, as was the case in this study, then it would experience the applied load for much longer periods than a near-surface inclusion on a cone raceway. The aforementioned discussion emphasizes the need to scan ultrasonically both the bearing cup (outer ring) raceways as well as the cone (inner ring) raceways. Moreover, the spalls that developed on test cups and cones at regions that did not match the locations of identified near-surface inclusions underscore the possible need to adjust the depth of the scans from the surface in order to capture relevant inclusions that might be a little deeper beyond the expected maximum Hertzian contact stress region ( $\sim 200 \mu\text{m}$ ).

Finally, these service life tests highlight the importance of steel cleanliness for tapered-roller bearing production. Bearing steels are already made to a higher quality than general grade steels, but low overall inclusion rates in bearing grade steels does not guarantee that the inclusions which do exist will not end up in the rolling contact fatigue (RCF) zone. Currently, the ASTM standards for bearing quality steels clearly have limitations with respect to guaranteeing the steel quality of bulk materials. New ultrasonic inspection techniques, such as the ones applied in this study, are necessary in order to address these shortcomings. These facts have

been the driving motivation behind the previous work done by the authors in this field, and are the continuing motivation to take the technology further, as shown by this study. Additionally, these results accentuate the need to use advanced ultrasonic techniques, such as surface wave scanning as a quality control tool for true fatigue resistant bearings.

## Acknowledgments

Special thanks to Amsted Rail's bearing division, BRESCO, for providing us the opportunity to work on this project and to Amsted Rail for funding the research.

## References

- [1] M.G. Dick, B.M. Wilson, "Roller Loads and Hertzian Contact Stress Modeling in Railcar Bearings Using Finite Element Analysis", Proceedings of the ASME RTD/TTCI Roller and Journal Bearing Symposium, Chicago, Illinois, September 11-12, 2007.
- [2] J.M. Beswick, "Bearing Steel Technology: Advances and State of the Art in Bearing Steel Quality Assurance", ASTM International, West Conshohocken, PA, 2007.
- [3] Y. Murakami, "Metal Fatigue: Effects of Small Defects and Nonmetallic Inclusions", Elsevier, Kidlington, Oxford, UK, pp. 75-159, 2002.
- [4] T.B. Lund, K. Törresvoll, "Quantification of Large Inclusions in Bearing Steel, Bearing Steel: Into the 21st Century", ASTM International, pp. 27-38, 1998.
- [5] H.K.D.H. Bhadeshia, "Steels for Bearings", Progress in Materials Science, Vol. 57, pp. 268-435, 2012.
- [6] ASTM A388/A388M-11, "Standard Practice for Ultrasonic Examination of Steel Forgings", Annual Book of ASTM Standards, Vol. 01.05, ASTM International, West Conshohocken, PA, 2011.
- [7] ASTM Standard E 45-11, "Standard Test Method for Determining the Inclusion Content of Steel", Annual Book of ASTM Standards, Vol. 03.01, ASTM International, West Conshohocken, PA, 2011.
- [8] ASTM Standard E1245-03, "Standard Practice for Determining the Inclusion or Second-Phase Constituent Content of Metals by Automatic Image Analysis", Annual Book of ASTM Standards, Vol. 03.01, ASTM International, West Conshohocken, PA, 2008.
- [9] ASTM Standard E2283-08, "Standard Practice for Extreme Value Analysis of Nonmetallic Inclusions in Steel and Other Microstructural Features", Annual Book of ASTM Standards, Vol. 03.01, ASTM International, West Conshohocken, PA, pp. 1341-1351, 2009.
- [10] ISO 4967, "Determination of Content of Nonmetallic Inclusions – Micrograph Method Using Standard Diagrams", Methods of Testing, TC 17, American National Standards Institute, 1998.
- [11] U. Zerbst, K. Madler, H. Hintze, "Fracture Mechanics in Railway Applications - An Overview", Engineering Fracture Mechanics, Vol. 72, pp. 163-194, 2005.

- [12] L. Koester, C. Zuhlke, D. R. Alexander, A. J. Fuller, B. M. Wilson, and J. A. Turner, "Near-race ultrasonic detection of subsurface defects in bearing rings," J. ASTM Int. STP1548, West Conshohocken, PA, pp. 84-101, 2012.
- [13] C. Tarawneh, L. Koester, A. J. Fuller, B. M. Wilson, J. A. Turner, "Service Life Testing of Components with Defects in the Rolling Contact Fatigue Zone", ASTM International, STP 1548, West Conshohocken, PA, pp. 67-83, 2012.
- [14] C. Tarawneh, J.A. Kypuros, A.A. Fuentes, B.M. Wilson, B.A. Gonzalez, G. Rodriguez, R.K. Maldonado, "Vibration Signatures of Temperature Trended Bearings in Field and Laboratory Testing", Proceedings of the ASME RTD Fall Technical Conference, RTDF2009-18038, Ft. Worth, Texas, October 20-21, 2009.
- [15] C. Tarawneh, A. A. Fuentes, J. A. Kypuros, L. A. Navarro, A. G. Vaipan, B. M. Wilson, "Thermal modeling of a railroad tapered roller bearing using finite element method", Journal of Thermal Science and Engineering Applications, Vol. 4, No. 3, pp. 9-19, 2012.